A thermo fluid dynamic model of wood particle gasification- and combustion processes

Gernot Boiger
ICP Institute of Computational Physics, School of Engineering, Zurich University of Applied Sciences, Wildbachstrasse 21, P.O. Box, 8401 Winterthur, Switzerland. gernot.boiger@zhaw.ch

ABSTRACT

In order to qualitatively understand and evaluate the thermo- fluid dynamic situation within a wood gasification reactor, a 1D particle model has been created. The presented tool accounts for the highly in- stationary, kinetic- and thermo chemical effects, leading to partial gasification and combustion of a wood particle embedded within a packed bed collective. It considers the fluid- dynamic situation within the changing porous bulk structure of the packed bed, its impact on species- and heat transition mechanisms, the energy- and mass balances of wood, coal, pyrolysis-gas, wood- gas and off- gas phases, the thermodynamics of locally developing gasification- and combustion reaction equilibria, as well as the presence of the chemical species hydrogen, water, carbon (di-) oxide, methane, oxygen, solid carbon and gaseous, longer chain hydrocarbons from pyrolysis.

Model results can be shown to yield very good, qualitative agreement with measurements, found in literature.

Keywords: Gasification, combustion, thermo chemistry, fluid dynamic, modelling

NOMENCLATURE

A'_{pyro}	Pre exponential factor wood pyrolysis (s^{-1})	**Greek Symbols**	
$A_{P,A}$	Cross section of process air cylinder (m^2)	α_G	Ratio of molar pyrolysis gas production rate to total pyrolysis rate (-)
$A_{WG,i}$	Frontal area of conical torch i (m^2)	α_j	Ratio of reacting component or species j total production rate of j (-)
A_g	Area of regional border plane g (m^2)	δ	Boundary layer thickness (m)
$C_{P,A}$	Lateral length of process air cube (m)	ε_{PB}	Packed bed porosity (-)
$c^{T_l}_{p,j}$	Heat capacity of species j at constant pressure and temperature T_1 (J/K mol)	ε_{coal}	Coal porosity (-)
D_P	Particle diameter (m)	η_A	Kinematic viscosity of process air (m^2/s)
D_{pore}	Coal pore diameter (m)	λ	Heat conduction coefficient (W/m K)

$D_{Diff,j}$	Diffusion coefficient of species j in air (m^2/s)
E'_{pyro}	Activation energy wood pyrolysis (J/mol)
f_{BN}	Bottle neck factor (-)
$\Delta h^{\Theta}_{f,j}$	Standard molar enthalpy of formation (J/mol)
$k_{\delta}^{l,l+1}$	Boundary layer coefficient between zones l and l+1 (m)
Δl_{pores}	Medium distance between pores (m)
MM_j	Molar mass of component or species j (kg/mol)
$N_{pores,P}$	Number of coal pores at particle surface (-)
N_j	Total number of molecules of species j within a balance zone (mol)
$\dot{n}_A^0$	Molar flux of incoming fresh air into particle vicinity (mol/s)
$\dot{n}_C^{Pyro}$	Rate of pyrolized carbon atoms (mol/s)
$\dot{n}_C^{Coal}$	Rate of molar coal production (mol/s)
$\dot{n}_C^{PG}$	Rate of molar pyrolysis gas production (mol/s)
$\dot{n}_{GP}$	Molecular species source term (mol/s m^3)
$\vec{n}_p$	Particle surface normal vector at pore (-)
$\dot{n}_{R,j}$	Reaction rate of species j (mol/s m^3)
$n_{g,i}$	Surface normal vector component of plane g (-)
p^{Θ}	Pressure at standard conditions (Pa)
$\dot{Q}_A$	Energy flux over plane in air phase (W)
R	Universal gas constant (J/K mol)
Re_{BN}	Bottle neck Reynolds number (-)
R_p	Radius of particle (m)
R_W	Radius of wooden particle core (m)
$R_{WG,PG}$	Ratio of molar wood gas to pyrolysis gas production (-)
$\overline{r}_{WG}$	Medium Radius of wood gas bubble (m)
T_l	Temperature of balance zone or component l (K)
T^{Θ}	Standard temperature (K)
v_A^{BN}	Process air velocity at bottle neck (m/s)
v_A^g	Process air velocity in zone g (m/s)
v_{WG}^P	Wood gas velocity at particle surface (m/s)
V_P	Particle volume (m^3)
$\dot{V}_j$	Volumetric flow rate of component j (m^3/s)
x_j	Molar fraction of component or species j (-)
x_i	Direction (-)
$x_{O_2}^{A,\Theta}$	Standard Oxygen content of process air (-)
ρ_j	Density of component j (kg/m^3)
$\gamma_{O/C}$	Ratio of O to C atoms in fuel (-)
$\gamma_{H/C}$	Ratio of H to C atoms in fuel (-)
ϑ_G^{Θ}	Molar gas density at standard conditions (mol/m^3)
$\vartheta_G^{T,p}$	Molar gas density at temperature T and pressure p (mol/m^3)

Superscripts

PEP	Pseudo Equilibrium Phase
TGP	Total Gas Production Phase
TPP	Total Product Phase

Subscripts

i	Alternatively: direction, time step, iteration, number of pore
BN	Bottle neck
A	Process air
P	Particle
GP	Gas production
W	Wood
coal	Coal
j	Molecular species
k	Atomic species O, H, C
l	Balance zone
g	Regional border plane
PG	Pyrolysis gas
G	Gas
W*	Combined wood and wood gas phase

1. INTRODUCTION

Up to this day, medium- and large scale, packed bed gasification plants (see e.g. [1]), have proven to require a relatively high level of maintenance intensity in order to keep up continuous, stationary production. It is still common practice to adjust process parameters via "trial and error methods" to changing input conditions.

This points to the fact that there is yet a demand for a deeper understanding of the relevant thermo-, fluid dynamic sub-processes involved in wood gasification. Thus compact, fast and comprehensive models of the situation within a packed bed gasifier are still required.

In this work, one such thermo-, fluid dynamic model is being presented and laid out in detail. The model is an addition to the relatively large amount of gasification models, described in literature (see e.g. [2] and [4–6]).

Among previously published works, a rough distinction can be made:

- *Reactor models*, with a focus on global mass- and heat balances, as well as transport phenomena on the packed bed scale (e.g. [3–4]).
- *Single particle models*, with a more detailed resolution of particle based, sub-processes, such as drying, pyrolysis, coal and pore formation, gasification and combustion (e.g. [8–9]).
- *Kinetic models*, which focus on chemical reaction rates but tend to neglect physical transport mechanisms (e.g. [5–19]).

The tool, described in this paper, basically falls into the category of *single particle* approaches, but does not neglect the fluid mechanic and structural coupling to the surrounding packed bed. It focuses on the scale level of about 10^{-2} m. As shown in chapter 2, the model provides a detailed, 1D depiction of the life span of an individual, reacting pellet or wood chip, the involved thermo chemistry, transition kinetics of molecular species, coal- and pore structure formation mechanisms as well as relevant heat- and species balances. In addition (as pointed out in chapter 2.7), the model features a specifically tailored, iterative, numerical solver to handle the highly transient, thermo chemical situation within the wood gas phase and the pores of the coal phase. This solver does not only, as most other modeling approaches (e.g. [4], [12] and [13]), use a "Gibbs Energy Minimization Method", but allows the calculation of a "Pseudo Equilibrium Phase" (PEP), with *zero* Gibbs free energy. So far, particle moisture content, drying effects, as well as the potential influence of non-spherical shape effects and thermal interaction with neighboring particles is either strongly simplified or neglected.

In chapter 3 it will be shown that this implementation, though representing a compact, single particle perspective, can achieve very good qualitative correspondence with packed bed, experimental results, published in literature [7]. Moreover it will be demonstrated that the model can be used to reinterpret certain, experimental results [7]. Thus its potential for further application is proven.

Chapter 4 then points towards future efforts to incorporate this single particle approach into a full 3D Eulerian – LaGrangian code, based on OpenFOAM® (see [15–18]).

2. THE MODEL

In this chapter the thermo-, fluid dynamic principles and concepts behind the 1D, single particle, wood gasification model are laid out and explained step by step.

The most essential, mathematical modelling concepts, range from setting up sensible balance zones, realizing the fluid mechanic coupling between single particle and packed bed, over the calculation of pyrolysis kinetics, coal- and pore structure formation mechanisms to the modelling of species exchange kinetics and the full resolution of the thermo chemical situation in terms of gasification and combustion effects.

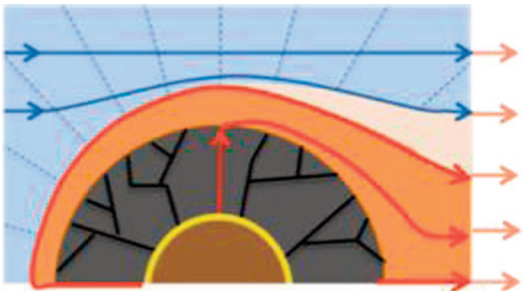

Figure 1: Wood gas (orange), off gas (pink), coal phase with pores (black) and pyrolysis zone (yellow); Red and orange streamlines represent wood gas and mixed product gas flow respectively

2.1 BALANCE ZONES AND COMPONENTS

The model distinguishes between four balance zones that transfer molecular species and energy between each other (see also Figure 1):

- The incoming, gaseous *process air phase*, with T_A^O ~ 300K, x_{O2}~ 0.21 and x_{N2}~ 0.79;
- The shrinking, solid *wood phase*, being processed by the protruding pyrolysis front;
- The produced, solid *coal phase* with pore structure;
- The produced, gaseous *wood gas phase*, which actually encompasses three kinds of gaseous mixtures, that are hereby referred to as *pyrolysis gas*, *wood gas* and *off gas*;

Pyrolysis gas is hereby regarded as a mixture of longer chain hydrocarbons, namely TARs, of which only the overall, atomic composition, is known. This composition corresponds to that of wood, according to $CO_{\frac{\gamma O}{C}} H_{\frac{\gamma H}{C}}$, but is enriched by oxygen and hydrogen, released by those cellulose components that turn into coal via pyrolysis.

Wood gas is the desired, but not exclusive product gas. Within the model, it is created out of *pyrolysis gas* by the gasification reactions (*thermo chemical stage 1*). Its composition remains to be calculated, but should range within the following limits (see [1]): CO (25%–45%), CO_2 (15%–30%), H_2O (g) (3%–20%), H_2 (15%–35%), CH_4 (4%–10%) and residual TARs (<3%).

Off gas is the undesired, but necessary by-product gas, created at the contact area between wood gas and process air. Within the model, it is created out of *wood gas* by combustion reactions (*thermo chemical stage 2*). It is composed of CO_2 and H_2O. The *off gas* production, via oxidation of *wood gas*, releases exothermal energy, which heats the entire particle system and keeps the thermo chemistry going.

2.2 COUPLING BETWEEN PARTICLE AND PACKED BED: MODELLING THE PROCESS AIR FLOW

Each particle is assigned a cubical region of process air phase with lateral length $C_{P,A}$ (see Equ.1), to account for packed bed porosity ε_{PB}, and a frontal, circular, cross section $A_{P,A}$ within the reactor (see Equ.2).

$$C_{P,A} = D_P * \sqrt[3]{\frac{\pi}{6*(1-\varepsilon_{PB})}} \qquad \text{Eqn. 1}$$

$$A_{P,A} = \frac{D_P^2 * \pi}{4} * \left(1 + 2 * f_{BN}^2\right) \qquad \text{Eqn. 2}$$

In Equ.2 a spherical particle bed structure is assumed. It allows for six *free flow bottleneck cross sections* per particle, where each has to be shared with two other, neighboring spheres. Each bottleneck cross section is assigned an approximate, representative diameter $f_{BN}*D_P$, such that f_{BN} is the *bottleneck factor*. In order to account for the over all porosity, f_{BN} is calculated as:

$$f_{BN} = \sqrt[3]{\frac{\varepsilon_{PB}}{1-\varepsilon_{PB}}} \qquad \text{Eqn. 3}$$

The velocity distribution of the stationary, compressible 1D gas flow with specific, molecular species source term n_{GP}, is simply derived by combining the 1D, inhomogeneous continuity equation, with the ideal gas law and the assumption that the cross sectional porosity approximately corresponds to the 3D porosity (see Equ.4).

$$\frac{\partial}{\partial x}\left[\frac{v_A^R(x)}{T(x)}\right] = \frac{\dot{n}_{GP}(x)*R}{p^{\Theta}*\varepsilon_{PB}} \qquad \text{Eqn. 4}$$

2.3 PYROLYSIS

The first thing that happens to the pre-heated particle (~700 K) is, that pyrolysis reactions set in at the surface of the spherical piece of fuel. Pyrolysis transforms the cellulose molecules into *pyrolysis gas* and *solid coal*. Thus, over time, a thickening coal layer is forming at the surface. The model particle diameter is shrinking, while the pyrolysis front is progressing towards the particle centre.

First the pyrolysis rate $\dot{n}_C^{Pyro}$, needs to be calculated in terms of pyrolized carbon atoms per time. A macroscopic *Arrhenius* approach, which averages over the entire particle, is chosen, according to [23], to implement the relevant kinetics:

$$\dot{n}_C^{Pyro} = A'_{pyro}*\left[\rho_P(x_W, x_{coal}, t) - \rho_{coal}\right]*V_P*MM_W^{-1}*e^{-\frac{E'_{pyrp}}{R*T_P(t)}} \qquad \text{Eqn. 5}$$

Equ.5 introduces the first, highly non-linear relationship to particle temperature T_p. Values for the activation energy E'_{pyro} and the pre exponential factor A'_{pyro}, have been taken out of [20]. The molar mass MM_W of one carbon atom, being assigned its pre-defined share of oxygen and hydrogen atoms, is calculated as:

$$MM_W = MM_C + \gamma_{O/C}*MM_O + \gamma_{H/C}*MM_H \qquad \text{Eqn. 6}$$

A certain fraction of pyrolized carbon atoms α_G, turns into *pyrolysis gas*, the rest turns into coal. Since coal mainly consists of solid carbon, all pyrolized oxygen and hydrogen atoms are going into the gas phase. With this definition and a user defined setting of α_G, coal and pyrolysis gas production rates can be calculated:

$$\dot{n}_C^{Coal} = (1-\alpha_G)*\dot{n}_C^{Pyro} \qquad \text{Eqn. 7}$$

$$\dot{n}_C^{PG} = \alpha_G*\dot{n}_C^{Pyro} \qquad \text{Eqn. 8}$$

2.4 COAL PORE STRUCTURE MODEL

With the assumption of a thickening coal layer, which covers the pyrolysis gas production front, the necessity arises to introduce a comprehensive coal pore structure model. Since the

velocity of the exiting wood gas at the particle surface v^{P}_{WG} is of interest, an approximation for the superficial coal pore area has to be developed.

Assuming isotropic coal porosity ε_{coal} and constant, circular coal pore cross sections of diameter D_{pore}, the following formulation for the number of pores N_{pores} at a radial distance r, from the particle center, has been derived:

$$N_{pores}(r) = \frac{16 * \varepsilon_{coal}}{3 * D_{pore}^2} * \left[(r + R_W)^2 - Rw * r \right] \qquad \text{Eqn. 9}$$

In Equ.9 the radius of the spherical, wooden particle core is included by R_W.

The volumetric flow rate $\dot{V}_{WG}$ of produced wood gas relates to the molar production rate of pyrolysis gas (Equ.10) via the molar production rate ratio $R_{WG,PG}$ and the ideal gas law, such that:

$$\dot{V}_{WG} = \dot{n}_C^{PG} * V_P * R_{WG,PG} * \frac{1}{\vartheta_G^{\Theta}} * \frac{T_{WG}}{T^{\Theta}} \qquad \text{Eqn. 10}$$

Combining Equ.9 and Equ.10 for $r = R_P$, with R_P being the total particle radius and $N_{pores,P} = N_{pores}(R_P)$, the velocity of exiting wood gas at the particle surface can then be calculated as:

$$v_{WG}^{P} = \frac{4 * \dot{V}_{WG}}{\pi * N_{pores,P} * D_{pore}^2} \qquad \text{Eqn. 11}$$

2.5 SIMPLIFIED FLUID MECHANICS OF THE INTERACTION BETWEEN PRODUCT GAS AND PROCESS AIR FLOW

Here a compact formulation for the contact area between the two gaseous balance zones, the *process air phase* and the *wood gas phase* is being proposed. Basically a 1D momentum balance between the incoming process air flow and the wood gas, protruding out of the particle, is being solved. In a first step, a representative *angle of process air attack* $\overline{\varphi}$ is calculated by *force effect averaging*, according to Eqn.12.

$$\overline{\varphi} = \arccos\left(\frac{1}{\pi}\right) \qquad \text{Eqn. 12}$$

Having defined $\overline{\varphi}$, the task of approximating the contact area can be reduced to a 0D problem. At this point the idea of an average, representative *wood gas protrusion radius* $\overline{r}_{WG}$ is formulated. This radius corresponds to the sum of the wood core radius R_W and the length of a representative pyrolysis gas/wood gas stream line, which starts at the pyrolysis front, goes along the very center of a straight coal pore and stops at the contact area to the *process air phase*. Then the assumption of three fluid dynamic *stages* is introduced: the *stable gas bubble stage* (*stage 1*), the gas *bubble break up stage* (*stage 2*) and the *air into pores stage* (*stage 3*). Within each stage, different physical conditions need to be taken into account and therefore the outflow radius needs to be calculated differently as well. Table 1 provides an overview of basic ideas, conditions and calculation methods for the three stages. Table 2 gives additional variables for calculations presented in Table 1, which are not laid out under section "Nomenclature". Consequentially, Figure 2 gives a more qualitative impression of how *stages 1-3* are distinguished at the pore scale level. Furthermore Figure 2 sketches the relevant oxygen transition areas between process air phase and wood gas phase, for all three stages.

Table 1: Basic ideas, conditions and calculations behind fluid dynamic stages 1-3

#	Basic idea	Condition(s)	$\overline{r}_{WG}$ *in m*
1	Particle engulfed by stable gas bubble	$\sum_{i=1}^{N_{pores,P}} A_{WG,i}\left(r_{WG,i}\right) \geq 4 * \overline{r_{WG}}^{2} * \pi$	$\left(\frac{\dot{V}_{WG} * \varepsilon_{PB}}{v_A^0 * \cos(\overline{\varphi}) * \pi}\right)^{\frac{1}{2}} * \left(\frac{MM_{WG} * T_{WG}}{MM_A * T_A}\right)^{\frac{1}{4}}$
2	Gas bubble break up after reduction of gas production rates	$\sum_{i=1}^{N_{pores,P}} A_{WG,i}\left(r_{WG,i}\right) < 4 * \overline{r}_{WG}^{2} * \pi$ $\wedge$ $\overline{r}_{WG} \geq R_P$	$R_P + k_\delta^{A,WG} * \sqrt{\frac{\dot{V}_{WG}}{N_{pores,P} * \pi * \Delta l_{pores} * \eta_A}} * \left\{ \begin{array}{l} \log\left[\frac{1+\sqrt{1+\overline{\Upsilon}_{A,WG}}}{\sqrt{\overline{\Upsilon}_{A,WG}} * \left(1+\sqrt{2}\right)}\right] \\ -\frac{1}{\sqrt{1+\overline{\Upsilon}_{A,WG}}} + \sqrt{\frac{\mathrm{P}_{A,WG}}{1+\mathrm{P}_{A,WG}}} \end{array} \right\}$
3	Air penetrates into pores shortly before extinction	$\overline{r}_{WG} < R_P$	$\sqrt[3]{\frac{1}{18} * \overline{\mathrm{H}}_{A,WG}} + \sqrt[3]{\frac{2}{3 * \overline{\mathrm{H}}_{A,WG}}} * \overline{\mathrm{K}}_{A,WG}^{3}$

Table 2: Variable definitions in addition to Table 1

Stage #	Symbol	Calculation	Unit
2	$\overline{\Upsilon}_{A,WG}$	$\frac{v_A^R * \cos(\overline{\varphi})}{v_{WG}^P}$	-
2	$\mathbf{P}_{A,WG}$	$\sqrt{\frac{\rho_A}{\rho_{WG}}} \approx \sqrt{\frac{T_{WG}}{T_A}}$	-
3	$\overline{\mathrm{K}}_{A,WG}$	$\frac{3 * \dot{V}_{WG}}{4 * \pi * \varepsilon_{coal} * P_{A,WG} * v_A^R * \cos(\overline{\varphi})}$	m^2
3	$\overline{\Gamma}_{A,WG}$	$R_W * \left(\overline{\mathrm{K}}_{A,WG} - R_W^2\right)$	m^3
3	$\overline{\mathrm{H}}_{A,WG}$	$-9 * \overline{\Gamma}_{A,WG} + i\sqrt{12 * \overline{\mathrm{K}}_{A,WG}^{3} - 81 * \overline{\Gamma}_{A,WG}^{2}}$	m^3

Even though the calculation of $\overline{r}_{WG}$ in stage 3 involves complex number mathematics, with $i=\sqrt{-1}$, the result proves to be a real number.

2.6 MASS AND HEAT TRANSFER

The four balance zones: *wood phase*, *coal phase*, *process air phase* and *wood gas phase* have been introduced in 2.1. They interact through momentum-, mass- and, heat transfer. In this work the emphasis lies on the latter two effects. Those are described by setting up coherent (atomic) species balances and sub models for the calculation of species transition kinetics.

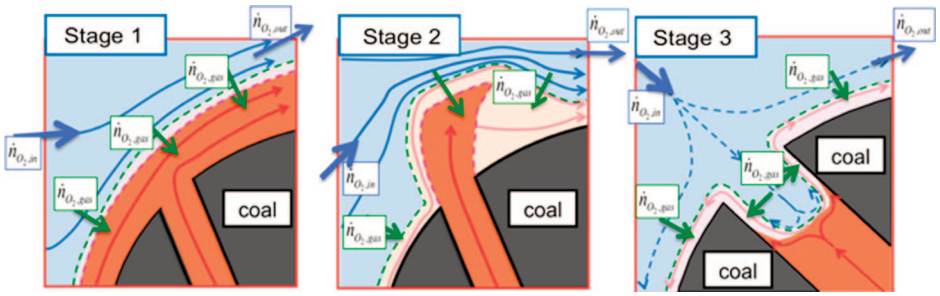

Figure 2: Sketch of model assumption for three stages of "fluid momentum interaction" at pore scale, between process air (blue), wood gas (orange) and oxidized off gas (pink). Red, pink and (dashed) blue lines represent wood gas, off gas and air streamlines respectively. Dashed green lines represent the oxygen transition area between the *process air zone* and the *wood gas zone*

2.6.1 Atomic species balances and species transition kinetics

The relevant, differential, conservative atomic species balance in tensor notation is shown in Eqn.13. This formulation encompasses all relevant (sub-) balance zones (l= wood-, coal-, process air-, wood gas phase, *pseudo equilibrium phase* PEP, *total gas phase* TGP and *total product phase* TPP), directions (i= 1; x_1= x), molecular species (j= CO, CO_2, H_2, H_2O, CH_4 and TARs) and atomic species (k= O, H, C). In stationary, convective, diffusive and chemical reaction effects are considered. The count of atoms of species k, per molecular species j is written as γ_k^j, while the species diffusion coefficient is $D_{Diff,j}$ and the specific and total molar species reaction rate within phase l are $\dot{n}_{R,j}^l$ and $\dot{N}_{R,j}^l$ respectively. The molecular species-specific coefficient α_j represents an essential modeling concept and gives the fraction of a certain species j that takes part in chemical reactions and is thus present within a sub- balance zone, namely the PEP (see 2.6.1). Note that x with subscript j signifies the molar fraction of a species j and x with a subscript i denotes any direction.

$$\gamma_k^j * \left[\frac{\partial n_j^l}{\partial t} + \alpha_j * \left(\frac{\partial x_j^l}{\partial x_i} * v_l^R * \vartheta_G^{T,p} + D_{Diff,j} * \frac{\partial^2 x_j^l}{\partial x_i^2} - \dot{n}_{R,j}^l \right) \right] = 0 \qquad \text{Eqn. 13}$$

2.6.1.1 Atomic species balances within "pseudo equilibrium phase", "total gas phase" and "total product phases"

Three sub-balance zones are introduced: the pseudo equilibrium phase PEP, the total gas phase TGP and the total product phase TPP. While TPP simply encompasses all gasification products, including coal, TGP holds only the sum of the gaseous products. PEP is more delicate. In order to create the PEP, the model postulates the existence of a locally stable chemical state of equilibrium, which has a Gibbs free energy equal to *zero*. This is only possible if the locally available, molecular species are not fully mixed and certain species remain *unprocessed*. While all gaseous species together form the TGP, the reacting species in their "pseudo equilibrium state" of Gibbs free energy equal to *zero*, form the PEP. Note that α_G is the ratio of pyrolysis gas production rate to total pyrolysis rate and is thus not to be mistaken for α_j.

In Table 3, specializations of Eqn.13 are presented, which account for the molecular species balances within the three sub zones. For reasons of mathematical practicality, balance ratios are used, rather than single-species-balances. Table 4 provides additional definitions of variables, used in Table 3.

Table 3: Species balance ratios for PEP, TGP, TPP

Zone	Balance ratio	Species input side	Species output side
PEP	$R^{PEP}_{O/C}$	$\frac{\gamma_{O/C} * \left(1-\alpha_G+\alpha_G * \alpha_{PG}+2 * \alpha_{O_2} * \gamma^{A,WG}_{O_2} / \gamma_{O/C}\right)}{\alpha_G * \alpha_{PG}+\alpha_{coal} * \gamma^{Coal,WG}_C}$	$\frac{2 * x^{PEP}_{O_2}+x^{PEP}_{H_2O}+2 * x^{PEP}_{CO_2}+x^{PEP}_{CO}}{x^{PEP}_{CO_2}+x^{PEP}_{CO}+x^{PEP}_{CH_4}}$
PEP	$R^{PEP}_{H/C}$	$\gamma_{H/C} * \left(\frac{1-\alpha_G+\alpha_G * \alpha_{PG}}{\alpha_G * \alpha_{PG}+\alpha_{coal} * \gamma^{Coal,WG}_C}\right)$	$2 * \frac{x^{PEP}_{H_2}+x^{PEP}_{H_2O}+2 * x^{PEP}_{CH_4}}{x^{PEP}_{CO_2}+x^{PEP}_{CO}+x^{PEP}_{CH_4}}$
TGP	$R^{TGP}_{O/C}$	$\frac{\gamma_{O/C}+2 * \gamma^{A,WG}_{O_2}}{\alpha_G+\gamma^{Coal,WG}_C}$	$\frac{2x^{PEP}_{O_2}+x^{PEP}_{H_2O}+2x^{PEP}_{CO_2}+x^{PEP}_{CO}+2X^{TGP}_{O_2}+\gamma_{O/C} * X^{TGP}_{CO\gamma_{O/C}H\gamma_{H/C}}}{x^{PEP}_{CO_2}+x^{PEP}_{CO}+x^{PEP}_{CH_4}+X^{TGP}_{CO\gamma_{O/C}H\gamma_{H/C}}}$
TGP	$R^{TGP}_{H/C}$	$\frac{\gamma_{H/C}}{\alpha_G+\gamma^{Coal,WG}_C}$	$\frac{2 * x^{PEP}_{H_2}+2 * x^{PEP}_{H_2O}+4 * x^{PEP}_{CH_4}+\gamma_{H/C} * X^{TGP}_{CO\gamma_{O/C}H\gamma_{H/C}}}{x^{PEP}_{CO_2}+x^{PEP}_{CO}+x^{PEP}_{CH_4}+X^{TGP}_{CO\gamma_{O/C}H\gamma_{H/C}}}$
TPP	$R^{TPP}_{O/C}$	$\gamma_{O/C}+2 * \gamma^{A,WG}_{O_2}$	$\frac{2 * x^{PEP}_{O_2}+x^{PEP}_{H_2O}+2 * x^{PEP}_{CO_2}+x^{PEP}_{CO}+2 * X^{TGP}_{O_2}+\gamma_{O/C} * X^{TGP}_{CO\gamma_{O/C}H\gamma_{H/C}}}{x^{PEP}_{CO_2}+x^{PEP}_{CO}+x^{PEP}_{CH_4}+X^{TGP}_{CO\gamma_{O/C}H\gamma_{H/C}}+X^{TPP}_{Coal}}$
TPP	$R^{TPP}_{H/C}$	$\gamma_{H/C}$	$\frac{2 * x^{PEP}_{H_2}+2 * x^{PEP}_{H_2O}+4 * x^{PEP}_{CH_4}+\gamma_{H/C} * X^{TGP}_{CO\gamma_{O/C}H\gamma_{H/C}}}{x^{PEP}_{CO_2}+x^{PEP}_{CO}+x^{PEP}_{CH_4}+X^{TGP}_{CO\gamma_{O/C}H\gamma_{H/C}}+X^{TPP}_{Coal}}$

Table 4: Variable definitions in addition to Table 3.

Definition	Symbol	Calculation	Unit
Ratio of molar diffusion rate of O_2 from process air to wood gas phase to rate of pyrolized carbon atoms	$\gamma_{O_2}^{A,WG}$	$\frac{\dot{n}_{O_2}^{A,WG}}{\dot{n}_C^{Pyro}}$	mol O_2/mol pyro
Ratio of molar coal reduction rate to rate of pyrolized carbon atoms	$\gamma_C^{Coal,WG}$	$\frac{\dot{n}_C^{Coal,WG}}{\dot{n}_C^{Pyro}}$	mol coal/mol pyro
Molar rate of non-reacting PG per total PEP production rate	$X_{CO\gamma_{O/C}H\gamma_{H/C}}^{TGP}$	$\frac{(1-\alpha_{PG})*\alpha_G*\dot{n}_C^{Pyro}}{\dot{n}_{tot}^{PEP}}$	mol PG/mol PEP
Molar rate of non-reacting O_2 per total PEP production rate	$X_{O_2}^{TGP}$	$\frac{(1-\alpha_{O_2})*(\alpha_G*\gamma_{O/C}*\dot{n}_C^{Pyro}+\dot{n}_{O_2}^{A,WG})}{\dot{n}_{tot}^{PEP}}$	mol O_2/mol PEP
Molar rate of produced coal to total PEP production rate	X_{Coal}^{TPP}	$\frac{(1-\alpha_K)*(1-\alpha_G)*\dot{n}_C^{Pyro}}{\dot{n}_{tot}^{PEP}}$	mol coal/mol PEP

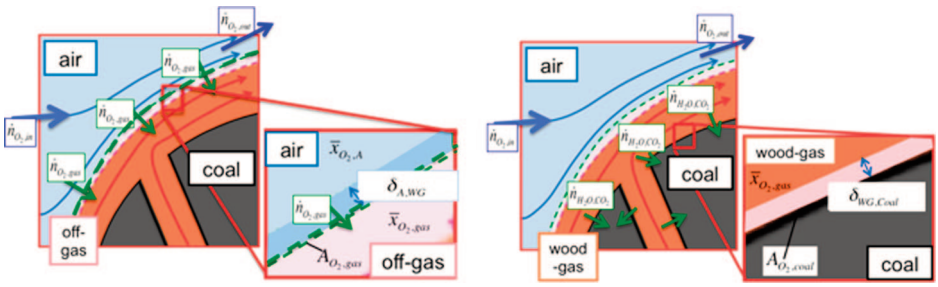

Figure 3: Sketch of model assumption for species transition situation during fluid dynamic *stage 1.* Zoomed in on boundary layer level. Green arrows represent species transition rate vectors. Dashed green lines (l) represent oxygen transition area between process air and wood gas $A_{A,WG}$. Straight black lines represent transition area between wood gas and coal surface $A_{WG,coal}$

2.6.1.2 Species transition kinetics: process air phase – wood gas phase – coal phase

A qualitatively valid approximation for species transition rates between the balance zones is needed. The two relevant species transfer mechanisms are O_2 transfer from *process air phase* to *wood gas phase* (see Figure 3, (l)) and transfer of H_2O (g) and CO_2 from *wood gas phase* to the coal surface (see Figure 3, (r)). Figure 3 sketches out the basic model assumption for implementing the species transition situation of O_2 (l) and H_2O plus CO_2 (r).

Thus the two main transition regions within the particle vicinity are the contact area between the *process air phase* and the *wood gas phase* $A_{A,WG}$ as well as the contact area between *wood gas phase* and *coal phase* $A_{WG,coal}$. Both values are coupled to the fluid dynamic interaction model introduced in chapter 2.5 and must be calculated differently as the fluid dynamic situation enters *stages 1-3*. Table 5 sums up the various transition-area formulations for *stages 1-3* and Table 6 provides additional variable definitions.

Now the diffusion boundary layer thicknesses $\delta_{A,WG}$ and $\delta_{WG,coal}$ for both transition mechanisms need to be approximated in order to get a hold on species transition coefficients. A very simple approach, derived from Prandtl's boundary layer theory [10] is chosen to accomplish this (see Table 7).

With those pieces of information, the full species transition model, including transition rates and β-values can be derived. In this work the β variable is used to represent the ratio between transition rates of species j from balance zone l to l+1, compared to the total molar inlet rates of species j into balance zone l. The remaining parts of the *species transition model* are laid out in Table 7 and Table 8.

2.6.2 Energy balances

The relevant, differential, conservative energy balance in tensor notation is shown in Eqn.14. This formulation encompasses all relevant balance zones (l= wood-, coal-, process air-, wood gas phase), directions (i= 1; x_1= x) and molecular species (j= CO, CO_2, H_2, H_2O, CH_4 and TARs). Heat transport phenomena are considered via convective and diffusive fluxes of molecular species and by heat conduction effects. Heat transition to other zones is derived from the heat conduction formulation, where λ_l is the heat conduction coefficient within zone l. The contribution of radiation heat exchange is left out because it is mostly relevant during the omitted heat up stage. Chemical energy release and in-stationary effects are considered

Table 5: Species transition area calculation, derived from fluid-dynamic model according to 2.5

Transition mechanism	Stage	Symbol	Calculation
Air-> O_2 -> Wood Gas	1, Stable gas bubble	$A_{A,WG}^{Stage1}$	$4*\overline{r}_{WG}^{2}*\pi$
Air-> O_2 -> Wood Gas	2, Bubble break up	$A_{A,WG}^{Stage2}$	$\sum_{i=1}^{N_{pores,P}} A_{WG,i}+\frac{\pi}{2}*\left(D_{WG,i}+D_{pore}\right)*\left(\overline{r}_{WG}-r_P\right)$
Air-> O_2 -> Wood Gas	3, Pore penetration	$A_{A,WG}^{Stage3}$	$A_P-A_{pores,P}+\frac{16*\varepsilon_{coal}*\pi}{3*d_{pore}^{2}}*\left[\frac{1}{3}*\left(\overline{r}_{WG}^{3}+r_P^{3}\right)+\frac{1}{2}*r_W*\left(r_P^{2}-\overline{r}_{WG}^{2}\right)+r_W^{2}*\left(r_P-\overline{r}_{WG}\right)\right]$
Wood Gas -> H_2O/CO_2 -> Coal	1, Stable gas bubble	$A_{WG,Coal}^{Stage1,2}$	$A_p-A_{pores,P}$
Wood Gas -> H_2O/CO_2 -> Coal	2, Bubble break up	$A_{WG,Coal}^{Stage1,2}$	$A_p-A_{pores,P}$
Wood Gas -> H_2O/CO_2 -> Coal	3, Pore penetration	$A_{WG,Coal}^{Stage3}$	$A_P-A_{pores,P}+\frac{16*\varepsilon_{coal}*\pi}{3*d_{pore}^{2}}*\left[\frac{1}{3}*\left(\overline{r}_{WG}^{3}+r_P^{3}\right)+\frac{1}{2}*r_W*\left(r_P^{2}-\overline{r}_{WG}^{2}\right)+r_W^{2}*\left(r_P-\overline{r}_{WG}\right)\right]$

Table 6: Variable definitions in addition to Table 5.

Definition	Symbol	Calculation	Unit
Ratio between process air speed component along the direction of surface normal vector of pore i to wood gas speed at pore outlet	$\gamma_{A,WG,i}$	$\frac{v_A^R*\cos(\varphi_i)}{v_{WG}^P}$	-
Square root of ratio between process air and wood gas densities, related to temperature difference within the two balance zones	$P_{A,WG}$	$\sqrt{\frac{\rho_A}{\rho_{WG}}}\approx\sqrt{\frac{T_{WG}}{T_A}}$	-
Frontal area of conical *wood gas* torch of pore i	$A_{WG,i}$	$\frac{A_{pore,P}}{\gamma_{A,WG,i}*P_{A,WG}}$	m^2
Diameter of $A_{WG,i}$	$D_{WG,i}$	$2*\sqrt{A_{WG,i}/\pi}$	m

Table 7: Species transfer model for O_2 from *air phase* to *wood gas phase* and H_2O or CO_2 from *wood gas phase* to coal surface.

Definition	**Symbol/Unit**	**Calculation**
Oxygen diffusion rate from *process air phase* to *wood gas phase*	$\dot{n}_{0_2}^{A,WG}$ /(mol /s)	$D_{Diff,O_2} * \frac{A_{A,WG}}{\delta_{A,WG}} * \vartheta_G^{\Theta} * \left(\overline{x}_{O_2}^{A} - \overline{x}_{O_2}^{WG}\right)$ $= \frac{D_{Diff,O_2}}{k_{\delta}^{A,WG}} * \sqrt{\frac{D_P * f_{BN} * v_A^0 * T_A^R}{\eta_A * \varepsilon_{PB} * T_A^0}} * A_{A,WG} * \vartheta_G^{\Theta} * \left(\overline{x}_{O_2}^{A} - \overline{x}_{O_2}^{WG}\right)$
Carbon-di-oxide and water diffusion rate from *wood gas phase* to *coal surface*	$\dot{n}_{H_2O,CO_2}^{WG,coal}$ /(mol/s)	$D_{Diff,H_2O,CO_2} * \frac{A_{WG,coal}}{\delta_{WG,coal}} * \vartheta_G^{\Theta} * \overline{x}_{H_2O,CO_2}^{WG}$ $= \frac{D_{Diff,H_2O,CO_2}}{k_{\delta}^{WG,coal}} * \sqrt{\frac{D_P * f_{BN} * v_A^0 * T_A^R}{\eta_A * \varepsilon_{PB} * T_A^0}} * A_{WG,coal} * \vartheta_G^{\Theta} * \overline{x}_{H_2O,CO_2}^{WG}$
Ratio of O_2 transition rate from air phase to wood gas phase to total fresh air O_2 supply rate	$\beta_{O_2}^{A,WG}$/ (-)	$\frac{f_A^{A,WG}}{\kappa_{Diff,O_2} * \sqrt{\frac{v_A^0 * T_A^0}{\varepsilon_{PB} * T_A^R}} + f_A^{A,WG}}$
Ratio of molar, $H_2O + CO_2$ transition rate from wood gas phase to coal phase to total $H_2O + CO_2$ production rate	$\beta_{H_2O,CO_2}^{WG,Coal}$/ (-)	$\frac{f_A^{WG,Coal}}{\gamma_{H_2O,CO_2;O_2}^{WG} * \kappa_{Diff,H_2O,CO_2} * \sqrt{\frac{v_A^0 * T_A^0}{\varepsilon_{PB} * T_A^R}} + f_A^{WG,Coal}}$

Table 8: Variable definitions in addition to Table 7.

Definition	Symbol	Calculation/Value	Unit
Ratio of molar $CO_2 + H_2O$ production rate by chemical reaction within wood gas phase to molar rate of total fresh air O_2 supply	$\gamma^{WG}_{H_2O,CO_2;O_2}$	$\frac{\dot{n}^{WG}_{R,H_2O+CO_2}}{\dot{n}^{A,0}_{O_2}}$	-
Approximate diffusion boundary layer thickness modeled according [10] for species transition from air to wood gas.	$\delta_{A,WG}$	$k^{A,WG}_{\delta} * \frac{1}{\sqrt{\mathrm{Re}_{BN}}}$	m
Approximate diffusion boundary layer thickness modeled according [10] for species transition from wood gas to coal.	$\delta_{WG,Coal}$	$k^{WG,Coal}_{\delta} * \frac{1}{\sqrt{\mathrm{Re}_{BN}}}$	m
Ratio of contact area between air phase and wood gas phase to reactor cross section per particle	$f^{A,WG}_{A}$	$A_{A,WG} / A_{P,A}$	-
Ratio of contact area between wood gas phase and coal phase to reactor cross section per particle	$f^{WG,Coal}_{A}$	$A_{WG,Coal} / A_{P,A}$	-
Inverse diffusion constant for O_2 diffusion	κ_{Diff,O_2}	$\frac{k^{A,WG}_{\delta}}{D_{Diff,O_2}} * \sqrt{\frac{\eta_A}{D_P * f_{BN}}}$	$s^{1/2}\,m^{1/2}$
Inverse diffusion constant for H_2O and CO_2 diffusion	κ_{Diff,H_2O,CO_2}	$\frac{k^{WG,coal}_{\delta}}{D_{Diff,H_2O,CO_2}} * \sqrt{\frac{\eta_A}{D_P * f_{BN}}}$	$s^{1/2}\,m^{1/2}$

as well. The molar enthalpy of formation of species j at standard pressure and balance zone temperature T_l is written as $\Delta h^{\Theta}_{f,j}(T_l)$. Other notations correspond to the formulation of the atomic species balance equation (see Eqn.13).

$$\frac{\partial\left(T_l * \vartheta_G^{T_l,p} * c^{T_l}_{p,j} * x^l_j\right)}{\partial t} + \frac{\partial\left(x^l_j * \nu^R_{j,i} * \vartheta_G^{T_l,p} + D_{Diff,j} * \frac{\partial x^l_j}{\partial x_i}\right) * c^{T_l}_{p,j} * T_l}{\partial x_i} + \lambda_l * \frac{\partial^2 T_l}{\partial x_i^2} - \dot{n}^l_{R,j} * \Delta h^{\Theta}_{f,j}(T_l) = 0 \qquad \text{Eqn. 14}$$

While the energy balances for the *wood gas phase*, the *wood*- and the *coal phase* are derived for a 0D domain, the process air phase balance is a 1D formulation.

2.6.2.1 Energy balance of air phase

For discretizing the process air phase angularly, along φ, a cylindrical coordinate system, with origin in the particle center, is introduced. For the solution of the energy balance, the corresponding 1D species balance needs to be solved first. The molecular species balance equation for the process air phase in its differential and numerical version is shown in Eqn.15 and Eqn.16 respectively. Hereby $\dot{n}_A^0$ is the molar flux of incoming fresh air into the entire particle vicinity with a standard concentration of $x_{O2}^{A,\Theta}$. Note that the indices i and j represent the temporal and spatial coordinate, respectively.

$$\frac{d\dot{n}_A(\varphi)}{d\varphi} = \frac{2*\dot{n}_A^0}{1+\cos(2\varphi)} - \frac{1}{2\pi} * \beta_{O_2}^{A,WG} * x_{O_2}^{A,\Theta} * \dot{n}_A^0 \qquad \text{Eqn. 15}$$

$$\dot{n}_A^{i,j}\left(\varphi^j\right) = \dot{n}_A^{i,j-1} + \frac{2*\dot{n}_A^0*\Delta\varphi}{1+\cos\left(2\varphi^j\right)} - \frac{1}{2\pi} * \beta_{O_2,i}^{A,WG} * x_{O_2}^{A,\Theta} * \dot{n}_A^0 * \Delta\varphi \qquad \text{Eqn. 16}$$

On basis of the species balance, the differential version of the process air, energy balance can be set up as shown in Eqn. 17.

$$\begin{aligned}&\frac{\partial T_A}{\partial t} + \frac{2*\pi}{N_A} * \dot{n}_A(\varphi) * \frac{\partial T_A}{\partial \varphi} = \\ &\frac{4*\pi*\Lambda_A}{1+\cos(2\varphi)} * T_A^0 + \Phi_{\lambda I}^{A,WG} * \sqrt{v_A^R} * T_{WG} \\ &\quad - \left[\frac{4*\pi*\Lambda_A}{1+\cos(2\varphi)} + 2*\beta_{O_2}^{A,WG} * x_{O_2}^{A,\Theta} * \Lambda_A + \Phi_{\lambda I}^{A,WG} * \sqrt{v_A^R}\right] * T_A(\varphi)\end{aligned} \qquad \text{Eqn. 17}$$

Introducing a numerical solution scheme for Eqn.17 and shifting the terms, such that the local process air temperature can be calculated, gives Eqn.18. Table 9 provides additional definitions of variables for Eqn.17 and Eqn.18.

$$\begin{aligned}&T_A^{i,j} = \\ &= \frac{1}{\Pi_A^{i,j}} * \left[\begin{array}{l}\frac{1}{\Delta t} T_A^{i-1,j} + \frac{2*\pi}{N_{A,i}*\Delta\varphi} * \dot{n}_A^{i,j} * T_A^{i,j-1} + \Phi_{\lambda I}^{A,WG} * \sqrt{v_A^R} * \left(T_{WG}^{i-1} - T_A^{i-1,j-1}\right) \\ + \frac{4*\pi*\Lambda_A^i}{\cos\left(2\varphi^j\right)+1} * \left(T_A^0 - T_A^{i-1,j-1}\right) + 2*\beta_{O_2,i}^{A,WG} * x_{O_2}^{A,\Theta} * \Lambda_A^i * T_A^0\end{array}\right]\end{aligned} \qquad \text{Eqn. 18}$$

2.6.2.2 Energy balance of wood-, product gas- and coal phase

From Eqn.17 the 0D, integrated energy balances of the combined *wood-* plus *wood gas phase* (denoted by index W*) and the *coal phase* can be derived. By shifting the terms, the temperature values of the balance zones can be calculated as seen in Eqn.19 and Eqn.20. Note that the index i represents the temporal co-ordinate and that the index j stands for chemical species in this context. Table 10 provides additional definitions of variables for Eqn.19 and Eqn.20.

Table 9: Variable definitions in addition to Eqn.17 and Eqn.18.

Definition	Symbol	Calculation/Value	Unit
Ratio between molar flux of incoming fresh air into the entire particle vicinity and total number of air molecules, already in vicinity	Λ_A	$\frac{\dot{n}_A^0}{N_A}$	1/s
Constant for ratio of diffusive heat flux to heat capacity within total process air phase	$\Phi_{\lambda I}^{A,WG}$	$\frac{A_{A,WG} * \vartheta_A^{\theta,T_A}}{k_\delta^{A,WG} * N_A * \mathrm{Pr}_A} * \sqrt{D_P * f_{BN} * \eta_A}$	$s^{-1/2}\ m^{-1/2}$
Prandtl number within process air phase	Pr_A	$\frac{c_{p,A}^{T_A} * \eta_A * MM_A * \vartheta^{\theta,T_A}}{\lambda_A}$	-
Average process air velocity within packed bed	v_A^R	v_A^0 / ε_{PB}	m/s
Constant for ratio of gross convective species flux into process air phase element j at time i to total number of molecules within that element	$\Pi_A^{i,j}$	$\frac{1}{\Delta t} + \frac{2 * \pi * \dot{n}_A^{i,j}}{N_{A,i} * \Delta\varphi}$	1/s

$$T_{W*}^{i} = T_{W*}^{i-1} * \left(1 - \frac{\Delta N_{W*}}{N_{W*}^{i-1}}\right) + \frac{\beta_{O_2,i}^{A,WG} * x_{O_2}^{A,\Theta} * \dot{n}_A^0}{N_{W*}^{i-1} * c_{p,W*}^{T_W}} * \left[\begin{array}{l} \left(T_A^{i-1} - \frac{\gamma_{C,O_2}^{Coal,WG}}{2} * T_{W*}^{i-1}\right) * \overline{c}_{p,O_2} + \gamma_{C,O_2}^{W} * \Delta h_W + \gamma_{C,O_2}^{Coal,WG} \\ * \left(\Delta h_{Coal} + c_{p,Coal}^{T_{W*}} * T_{Coal}^{i-1}\right) - \gamma_{C,O_2}^{Coal} * \left(\Delta h_{Coal} + c_{p,W}^{T_{W*}} * T_{W*}^{i-1}\right) - \\ -\gamma_{C,O_2}^{WG} * \sum_j \left[x_j^{WG} * \left(\Delta h_j^{WG} + x_j^{WG} * c_{p,j}^{T_{W*}} * T_{W*}^{i-1}\right)\right] \\ -\Phi_{\lambda II,i}^{A,WG} * \left(T_{W*}^{i-1} - T_A^{i-1}\right) - \Phi_{\lambda,\alpha,i}^{Coal,W*} * \left(T_{W*}^{i-1} - T_{Coal}^{i-1}\right) \end{array}\right] * \Delta t \qquad \text{Eqn. 19}$$

$$T_{Coal}^{i} = T_{Coal}^{i-1} * \left(1 - \frac{\Delta N_{Coal}}{N_{Coal}^{i-1}}\right) + \frac{\beta_{O_2,i}^{A,WG} * x_{O_2}^{A,\Theta} * \dot{n}_A^0}{N_{Coal}^{i-1} * c_{p,Coal}^{T_{Coal}}} * \left[\begin{array}{l} \gamma_{C,O_2}^{Coal} * c_{p,W}^{T_W} * T_W^{i-1} - \gamma_{C,O_2}^{Coal,WG} * c_{p,Coal}^{T_{Coal}} * T_{Coal}^{i-1} + \\ +\Phi_{\lambda III,i}^{Coal,WG} * \left(T_{WG}^{i-1} - T_{Coal}^{i-1}\right) + \Phi_{\alpha,i}^{Coal,W} * \left(T_W^{i-1} - T_{Coal}^{i-1}\right) \end{array}\right] * \Delta t \qquad \text{Eqn. 20}$$

2.7 THERMO CHEMISTRY MODEL

Within the entire gasification process, two zones of intense thermo chemical reactions play a major role besides the, previously discussed, pyrolysis zone:

- Thermo chemical stage 1: The gasification zone
- Thermo chemical stage 2: The combustion zone

Table 10: Variable definitions in addition to Eqn.19 and Eqn.20.

Definition	Symbol/Unit	Calculation
Coefficient of ratio between heat transition (coal phase - wood plus wood gas phase) to fresh air O_2 supply at time step i	$\Phi_{\lambda,\alpha,i}^{Coal,W*}$ / (J/K mol)	$\left(\frac{A_{Coal,W}^{i}}{A_{Coal,W}^{i}+A_{Coal,WG}^{i}}\right)*\frac{\alpha_{Coal,W}*A_{Coal,W}^{i}}{\beta_{O_2,i}^{A,WG}*x_{O_2}^{A,\Theta}*\dot{n}_{\boldsymbol{A}}^{0}}+\left(\frac{A_{Coal,WG}^{i}}{A_{Coal,W}^{i}+A_{Coal,WG}^{i}}\right)*\Phi_{\lambda II,i}^{Coal,WG}$
Ratio between heat transition (process air phase - wood gas phase) to fresh air O_2 supply at time step i	$\Phi_{\lambda II,i}^{A,WG}$/ (J/K mol)	$\frac{\lambda_A*A_{WG,A}^{i}*\sqrt{\mathrm{Re}_{BN}^{i}}}{k_{\delta}^{WG,A}*\beta_{O_2,i}^{A,WG}*x_{O_2}^{A,\Theta}*\dot{n}_{\boldsymbol{A}}^{0}}$
Ratio between heat transition (coal phase - wood gas phase) to fresh air O_2 supply at time step i	$\Phi_{\lambda III,i}^{Coal,WG}$ / (J/K mol)	$\frac{\lambda_A*A_{Coal,WG}^{i}*\sqrt{\mathrm{Re}_{BN}^{i}}}{k_{\delta}^{Coal,WG}*\beta_{O_2,i}^{A,WG}*x_{O_2}^{A,\Theta}*\dot{n}_{\boldsymbol{A}}^{0}}$
Ratio between heat transition (coal phase - wood phase) to fresh air O_2 supply at time step i	$\Phi_{\alpha,i}^{Coal,W}$ / (J/K mol)	$\frac{\alpha_{Coal,W}*A_{Coal,W}^{i}}{\beta_{O_2,i}^{A,WG}*x_{O_2}^{A,\Theta}*\dot{n}_{\boldsymbol{A}}^{0}}$
Ratio of molar coal transition rate to wood gas phase due to reduction to molar rate of total fresh air O_2 supply	$\gamma_{C,O_2}^{Coal,WG}$/ (-)	$\frac{\dot{n}_{C}^{Coal,WG}}{\dot{n}_{O_2}^{A,0}}$
Ratio of molar coal production rate to molar rate of total fresh air O_2 supply	γ_{C,O_2}^{Coal}/ (-)	$\frac{\dot{n}_{C}^{Coal}}{\dot{n}_{O_2}^{A,0}}$
Ratio of pyrolized carbon rate to molar rate of total fresh air O_2 supply	γ_{C,O_2}^{W}/ (-)	$\frac{\dot{n}_{C}^{Pyro}}{\dot{n}_{O_2}^{A,0}}$
Ratio of molar wood gas production rate to molar rate of total fresh air O_2 supply	γ_{C,O_2}^{WG}/ (-)	$\frac{\dot{n}_{j}^{WG}}{\dot{n}_{O_2}^{A,0}}$

Gasification and combustion zone are located within the *wood gas phase*. All relevant thermo chemical reactions take place there. The gasification zone is located in close proximity to the coal surface (including the pore structure) while the combustion zone occurs at the contact area between *wood gas phase* and *process air phase*.

For closer examination of the phenomena, three additional sub-zones have been introduced as description in chapter 2.6.1.

2.7.1 Thermo chemical stage 1: gasification model

The developed, thermo chemical model resolves the relevant, molecular species composition x_j for the three sub-zones: the PEP, the TGP and the TPP. Actually the gas composition within PEP x_j^{PEP} is resolved first. Within PEP, j = H_2O, H_2, CO, CO_2, CH_4 and O_2. The calculation is performed at each numerical time step, assuming that, within PEP a complete chemical equilibrium is formed. Therefore the time constants of the involved reaction kinetics have to be significantly smaller, than the chosen numerical time step Δt. By calculating x_j^{PEP}, the atomic species balance for PEP can be closed. Then the production rates of coal and non-reacting pyrolysis gas are calculated. Finally the atomic species balances for TGP and TPP can be closed as well (see Table 3).

2.7.1.1 Gasification reactions

A condensation of the most relevant thermo chemical gasification reactions, reveals three basic mechanisms (see e.g. [1]) that are assumed to exist in complete equilibrium within the *pseudo equilibrium phase*:

- The Boudouard reaction:

$$C(g/s) + CO_2 \xleftrightarrow{K_1} 2CO \qquad \text{Eqn. 21}$$

- The Methanation reaction:

$$C(g/s) + 2H_2 \xleftrightarrow{K_2} CH_4 \qquad \text{Eqn. 22}$$

- The Water gas shift:

$$C(g/s) + H_2O \xleftrightarrow{K_3} CO + H_2 \qquad \text{Eqn. 23}$$

Note the "(g/s)" notation. It hints to the fact that those reactions can occur both as heterogeneous mechanisms with the *coal phase* C(s) and as homogeneous reactions with pyrolized hydrocarbons within the pyrolysis gas C(g).

Even if no oxygen from the process air penetrates to the particle surface or the pyrolysis gas zone, oxygen will still be present to act as reactant for the formation of the PEP. Its origin is the pyrolized wood itself. Thus relevant oxidation reactions have to be included in the calculation of the gasification equilibrium as well, such that a fourth equilibrium reaction can be assumed:

- The oxidation reaction within the gasification zone

$$CH_4 + H_2 + CO + 3O_2 \xleftrightarrow{K_{10}} 2CO_2 + 3H_2O \qquad \text{Eqn. 24}$$

Note the constants of equilibria K_j in Eqn.21 – 24. They are sensitive to temperature and are calculated at each numerical time step. The procedure to obtain the constants of equilibria is well known (see [6], [11, 12]) and is hereby based on thermodynamic coefficients $a_{i,n}$ and $b_{i,n}$, published by NASA [14]. Table 11 sums up the implementation for obtaining K_j. Used indices i, j and n stand for molecular species, distinct, chemical reactions and the number of the individual, suitable coefficient from [14], respectively. In table 11, $\gamma_{i,j}$ are the stoichiometric coefficients of species i in reaction equation j.

Table 11: Procedure to obtain the equilibrium constant for reaction j: K_j (see also [11, 12]).

Step	Definition	Symbol/ Units	Calculation
1	Thermodynamic coefficient n for species i in reaction j, [14]	$a_{j,n}$	$\sum_i (\gamma_{i,j} * a_{i,n})$
2	Thermodynamic coefficient n for species i in reaction j, [14]	$b_{j,n}$	$\sum_i (\gamma_{i,j} * b_{i,n})$
3	Molar, standard enthalpy of reaction j	$\Delta h^{\Theta}_{R,j}$ /(J/mol)	$\left[\sum_{n=1}^{5} \left(a_{j,n} * \frac{T_{WG}^{n-1}}{n} \right) + \frac{b_{j,1}}{T_{WG}} \right] * R * T_{WG}$
4	Molar, standard entropy of reaction j	$\Delta s^{\Theta}_{R,j}$ /(J/mol)	$\left[a_{j,1} * \ln(T_{WG}) + \sum_{n=2}^{5} \left(a_{j,n} * \frac{T_{WG}^{n-1}}{n-1} \right) + b_{j,2} \right] * R$
5	Molar, standard Gibbs free energy of reaction j	Δg^{Θ}_{j} /(J/mol)	$\frac{\Delta h^{\Theta}_{j}(T_{WG})}{R * T_{WG}} - \frac{\Delta s^{\Theta}_{j}(T_{WG})}{R}$
6	Molar, Gibbs free energy of reaction j	Δg_j /(J/mol)	$\Delta g^{\Theta}_{j}(T_{WG}) + R * T_{WG} * \left[\ln\left(\frac{p * x_i}{p^{\Theta}} \right) \right] = 0$
7	Equilibrium constant of reaction j at T_{WG}	K_j/(-)	$e^{-\left[\Delta g^{\Theta}_{j}(T_{WG}) \right]}$

2.7.1.2 Unknowns and set of equations

The presented solution for the gasification chemistry within PEP is based upon the idea that, in addition to the six unknowns x_j^{PEP}, four α'_j values have to be found as well. For the calculation within PEP, j'= "G" (gas phase), PG (pyrolysis gas), coal and O_2. This makes a system of ten unknowns: $x_{H2O}^{PEP}, x_{H2}^{PEP}, x_{CO}^{PEP}, x_{CO2}^{PEP}, x_{CH4}^{PEP}, x_{O2}^{PEP}, \alpha_G, \alpha_{PG}, \alpha_{coal}, \alpha_{O2}$.

The equations and conditions for resolving this problem are presented in Table 12. They are based upon the assumption of chemical equilibrium for the gasification reactions, the over-all species balance and the H/C as well as O/C balance ratios for PEP.

2.7.1.3 Iterative gasification solver

An *iterative gasification solver* has been developed to solve the problem, posed in Table 12 for the *pseudo equilibrium phase*. In contrast to Gibbs energy minimization procedures, described e.g. in [13], it aims for *zero* Gibbs free energy and calculates fractions of potential reactants, that are available, but may not be involved in the reactions, in order to obtain this state. Table 13 lists the corresponding, iterative solution procedure, which is performed at each numerical time step. Note that in Table 13, index i denotes the iterative step.

Table 12: Equations and conditions for resolving thermo chemistry within PEP. Note that the super scripts for PEP are omitted in this table.

#	Name/Symbol	Equation/Condition
1	Boudouard	$K'_1 = \frac{1}{K_1} = \frac{x_{CO_2}}{x_{CO}^2}$
2	Methanation	$K_2 = \frac{x_{CH_4}}{x_{H_2}^2}$
3	Water gas shift	$K'_3 = \frac{1}{K_3} = \frac{x_{H_2O}}{x_{H_2} * x_{CO}}$
4	Oxidation	$K_{10} = \frac{x_{CO_2}^2 * x_{H_2O}^3}{x_{H_2} * x_{CO} * x_{CH_4} * x_{O_2}^3}$
5	Species balance	$x_{H_2O} + x_{H_2} + x_{CO_2} + x_{CO} + x_{CH_4} + x_{O_2} = 1$
6	O/C balance, $R_{O/C}^{PEP}$	$\frac{\gamma_{O/C} * \left(1 - \alpha_G + \alpha_G * \alpha_{PG} + 2 * \alpha_{O_2} * \gamma_{O_2}^{A,WG} / \gamma_{O/C}\right)}{\alpha_G * \alpha_{PG} + \alpha_K * \gamma_C^{Coal,WG}} - \frac{x_{CO} + 2x_{CO_2} + x_{H_2O} + 2x_{O_2}}{x_{CH_4} + x_{CO_2} + x_{CO}} = 0$
7	H/C balance, $R_{H/C}^{PEP}$	$\gamma_{H/C} * \left(\frac{1 - \alpha_G + \alpha_G * \alpha_{PG}}{\alpha_G * \alpha_{PG} + \alpha_K * \gamma_C^{Coal,WG}} \right) - \frac{4x_{CH_4} + 2x_{H_2O} + 2x_{H_2}}{x_{CH_4} + x_{CO_2} + x_{CO}} = 0$
8	α_G input	user input
9	α_{O2} restriction	$0 \le \alpha_{O2} \le 1$
10	α_{coal} restriction	$0 \le \alpha_{coal} \le 1$

2.7.2 Thermo chemical stage 2: combustion model

As postulated by the model, the *wood gas phase*, with compositions having been calculated by the gasification solver (see 2.7.1), hits the process air phase at the contact area $A_{A,WG}$, which in turn is calculated as described in Table 5. Oxygen reaches the *wood gas phase* via diffusive transport mechanisms (see Table 7). Thus combustion reactions occur in addition to the actual gasification. Here the combustion reactions are modeled to occur in combination with an intense, internal mixing of the *wood gas phase*. Consequentially it is assumed, that a global minimization of Gibbs free energy, within the entire *wood gas phase* takes place. The method of *LaGrangian multipliers* is used in order to obtain a state of global Gibbs energy minimization for all contributing *wood gas phase* components and gives the final product gas composition. The procedure is not depicted in detail here, since it is equivalent to methods published in literature e.g. [13].

Table 13: Equations and conditions for resolving thermo chemistry within PEP. Note that the super scripts for PEP are omitted in this table.

#	Step/Symbol	Equation/Condition
1	Estimate starting value for $x_{CO}^{PEP,i}$, using information from previous iterations	$\sum_{n=1}^{i=1} \frac{\Delta^n x_{CO}^{PEP,i-1-n}}{\Delta i^n} * \frac{1}{n!}$
2	Calculate $x_{H2}^{PEP,i}$	$\frac{1}{2*K_2} * \left\{ -K_{CO}^{PEP,i} + \sqrt{\left(K_{CO}^{PEP,i}\right)^2 - 4*K_2 * x_{CO}^{PEP,i} * \left[\left(K_1^{'} + K_{11}\right) * x_{CO}^{PEP,i} + 1 - \frac{1}{x_{CO}^{PEP,i}} \right]} \right\}$
	Insert $K_{CO}^{PEP,i}$	$1 + K_3^{'} * x_{CO}^{PEP,i}$
	Insert K_{11}	$K_3^{'} * \sqrt[3]{\frac{K_1^2}{K_2 * K_{10}}}$
3	Calculate $R_{O/C}^{PEP,i}$ using Table 1 and Eqn. 40 - 42	$\frac{x_{CO}^{PEP,i} + 2*K_1^{'} * \left(x_{CO}^{PEP,i}\right)^2 + K_3^{'} * x_{CO}^{PEP,i} * x_{H_2}^{PEP,i} + 2*K_{11} * \left(x_{CO}^{PEP,i}\right)^2}{K_2 * \left(x_{H_2}^{PEP,i}\right)^2 + K_1^{'} * \left(x_{CO}^{PEP,i}\right)^2 + x_{CO}^{PEP,i}}$
4	Calculate α_{O2}^{i}	$\frac{1}{2*\gamma_{O_2}^{A,WG}} * \left[R_{O/C}^{PEP,i} * \left(\alpha_G * \alpha_{PG}^{i-1} + \alpha_{coal}^{i-1} * \gamma_C^{Coal,WG}\right) + \gamma_{O/C} * \left(\alpha_G - 1 - \alpha_G * \alpha_{PG}^{i-1}\right) \right]$
5	Calculate α_{coal}^{i} if $\alpha_{O2}^{i}=0$ or $\alpha_{O2}^{i}=1$, else $\alpha_{coal}^{0}=1$;	$\frac{\gamma_{O/C} * \left(1 - \alpha_G + \alpha_G * \alpha_{PG}^{i-1} + 2*\alpha_{O_2}^{i-1} * \frac{\gamma_{O_2}^{A,WG}}{\gamma_{O/C}}\right) - \alpha_G * \alpha_{PG}^{i-1} * R_{O/C}^{PEP,i}}{R_{O/C}^{PEP,i} * \gamma_C^{Coal,WG}}$

(*Contd*)

Table 13: Equations and conditions for resolving thermo chemistry within PEP. Note that the super scripts for PEP are omitted in this table. (*Continued*)

#	Step/Symbol	Equation/Condition
6	Calculate α^{i}_{PG} if (α^{i}_{O2}=0 or α^{i}_{O2} =1) and (α^{i}_{coal}=0 or α^{i}_{coal}=1) else α^{0}_{coal}= "user defined";	$\frac{\gamma_{O/C} * \left(1-\alpha_G\right)+2*\alpha_{O_2}^{i} * \gamma_{O_2}^{A,WG} - \alpha_K^{i} * \gamma_C^{A,WG} * R_{O/C}^{PEP,i}}{\alpha_G * \left(R_{O/C}^{PEP,i} - \gamma_{O/C}\right)}$
7	Calculate $x_{CO}^{PEP,i*}$	$\frac{1}{2*R_{H/C}^{PEP,i} * K_1^{'}} * \left\{ -K_{H_2}^{PEP,i} + \sqrt{\left(K_{H_2}^{PEP,i}\right)^2 - 4 * R_{H/C}^{PEP,i} * K_1^{'} * \left[\left(R_{H/C}^{PEP,i} - 4\right) * K_2 - \frac{2}{x_{H_2}^{PEP,i}} \right] * \left(x_{H_2}^{PEP,i}\right)^2} \right\}$
	Insert $K_{H2}^{PEP,i}$	$R_{H/C}^{PEP,i} - 2 * K_3^{'} * x_{H_2}^{PEP,i}$
	Insert $R_{H/C}^{PEP,i}$	$\gamma_{H/C} * \left(\frac{1-\alpha_G+\alpha_G * \alpha_{PG}^{i}}{\alpha_G * \alpha_{PG}^{i} + \alpha_K^{i} * \gamma_C^{Coal,WG}} \right)$
8	Iterate step 1 to 7 to convergence	
9	Calculate remaining species in equilibrium with x_{CO}^{PEP} and x_{H2}^{PEP}	$x_{CO_2}^{PEP} = 2 * K_1^{'} * \left(x_{CO}^{PEP}\right)^2; \quad x_{H_2O}^{PEP} = K_3^{'} * x_{CO}^{PEP} * x_{H_2}^{PEP};$
		$x_{CH_4}^{PEP} = K_2 * \left(x_{H_2}^{PEP}\right)^2; \quad x_{O_2}^{PEP} = 2 * K_{11} * \left(x_{CO}^{PEP}\right)^2$
10	Check consistency of atomic species balance ratio for PEP $R_{H/C}^{PEP}$ (see Table 1)	$\gamma_{H/C} * \left(\frac{1-\alpha_G+\alpha_G * \alpha_{PG}}{\alpha_G * \alpha_{PG} + \alpha_K * \gamma_C^{Coal,WG}} \right) \overset{!}{=} 2 * \frac{x_{H_2}^{PEP} + x_{H_2O}^{PEP} + 2 * x_{CH_4}^{PEP}}{x_{CO_2}^{PEP} + x_{CO}^{PEP} + x_{CH_4}^{PEP}}$
	Check consistency of atomic species balance ratio for PEP, $R_{O/C}^{PEP}$ (see Table 1)	$\frac{\gamma_{O/C} * \left(1-\alpha_G+\alpha_G * \alpha_{PG} + 2 * \alpha_{O_2} * \gamma_{O_2}^{A,WG} / \gamma_{O/C}\right)}{\alpha_G * \alpha_{PG} + \alpha_K * \gamma_C^{Coal,WG}} \overset{!}{=} \frac{2 * x_{O_2}^{PEP} + x_{H_2O}^{PEP} + 2 * x_{CO_2}^{PEP} + x_{CO}^{PEP}}{x_{CO_2}^{PEP} + x_{CO}^{PEP} + x_{CH_4}^{PEP}}$

11 Calculate molar production rate of non- reacting pyrolysis gas $\dot{n}_{CH_{\frac{\gamma H}{C}}O_{\frac{\gamma O}{C}}}$

$$\left(1-\alpha_{PG}\right)*\alpha_G*\dot{n}_C^{pyro}$$

Check consistency of atomic species balance ratio for TGP $R_{H/C}{}^{TGP}$ (see Table 1)

$$\frac{\gamma_{H/C}}{\alpha_G+\gamma_C^{Coal,WG}}\overset{!}{=}\frac{2*x_{H_2}^{PEP}+2*x_{H_2O}^{PEP}+4*x_{CH_4}^{PEP}+\gamma_{H/C}*X_{CO\gamma_{O/C}H\gamma_{H/C}}^{TGP}}{x_{CO_2}^{PEP}+x_{CO}^{PEP}+x_{CH_4}^{PEP}+X_{CO\gamma_{O/C}H\gamma_{H/C}}^{TGP}}$$

Check consistency of atomic species balance ratio for TGP $R_{O/C}{}^{TGP}$ (see Table 1)

$$\frac{\gamma_{O/C}+2*\gamma_{O_2}^{A,WG}}{\alpha_G+\gamma_C^{Coal,WG}}\overset{!}{=}\frac{2x_{O_2}^{PEP}+x_{H_2O}^{PEP}+2x_{CO_2}^{PEP}+x_{CO}^{PEP}+2X_{O_2}^{TGP}+\gamma_{O/C}*X_{CO\gamma_{O/C}H\gamma_{H/C}}^{TGP}}{x_{CO_2}^{PEP}+x_{CO}^{PEP}+x_{CH_4}^{PEP}+X_{CO\gamma_{O/C}H\gamma_{H/C}}^{TGP}}$$

12 Calculate molar production rate of coal $\dot{n}_{C(s)}$

$$\left(1-\alpha_G\right)*\dot{n}_C^{pyro}(t)$$

Check consistency of atomic species balance ratio for TPP $R_{H/C}{}^{TPP}$

$$\gamma_{H/C}\overset{!}{=}\frac{2*x_{H_2}^{PEP}+2*x_{H_2O}^{PEP}+4*x_{CH_4}^{PEP}+\gamma_{H/C}*X_{CO\gamma_{O/C}H\gamma_{H/C}}^{TGP}}{x_{CO_2}^{PEP}+x_{CO}^{PEP}+x_{CH_4}^{PEP}+X_{CO\gamma_{O/C}H\gamma_{H/C}}^{TGP}+X_{Coal}^{TPP}}$$

Check consistency of atomic species balance ratio for TPP $R_{O/C}{}^{TPP}$

$$\gamma_{O/C}+2*\gamma_{O_2}^{A,WG}\overset{!}{=}\frac{2*x_{O_2}^{PEP}+x_{H_2O}^{PEP}+2*x_{CO_2}^{PEP}+x_{CO}^{PEP}+2*X_{O_2}^{TGP}+\gamma_{O/C}*X_{CO\gamma_{O/C}H\gamma_{H/C}}^{TGP}}{x_{CO_2}^{PEP}+x_{CO}^{PEP}+x_{CH_4}^{PEP}+X_{CO\gamma_{O/C}H\gamma_{H/C}}^{TGP}+X_{Coal}^{TPP}}$$

3. QUALITATIVE VERIFICATION AND RESULTS

This chapter focuses on a comparison of model outcome to data from literature and the presentation of further model results, produced for exemplary parameter combinations.

So far the experimental work, published by Fatehi and Kaviany [7], has been particularly helpful to prove the validity of the presented gasification model. The fact, that a remarkable, qualitative agreement between model results and experiments can be shown, proves that a single particle model can provide valuable information on the state of an entire packed bed reactor.

3.1 FLAME FRONT SPEED AGAINST PROCESS AIR SPEED

The first criterion for model validity can be obtained by investigating the experimentally obtained "flame front speed v_{FF} against process air speed v_A", derived from the fixed bed, up draft gasifier, seen in Figure 4 and published in [7].

Figure 4 shows a direct comparison between the 20-year old, experimental results from Fatehi and Kaviany, to equivalent results, obtained for two different sets of parameters (assuming pellets and wood chips as fuel), by the hereby presented model. The comparison reveals that an outstanding, qualitative agreement can be achieved. It proves that the model can produce sensible results over a wide range of oxygen/fuel ratios. Note that, in almost exact agreement with experiments, the model gives a process air speed of about 1 m/s that would lead to extinguishing the flame.

3.2 TEMPERATURE AT DIFFERENT HEIGHTS AGAINST TIME

The second kind of experimental evaluation, published in [7], is about mounting temperature sensors at various heights within the reactor and about monitoring

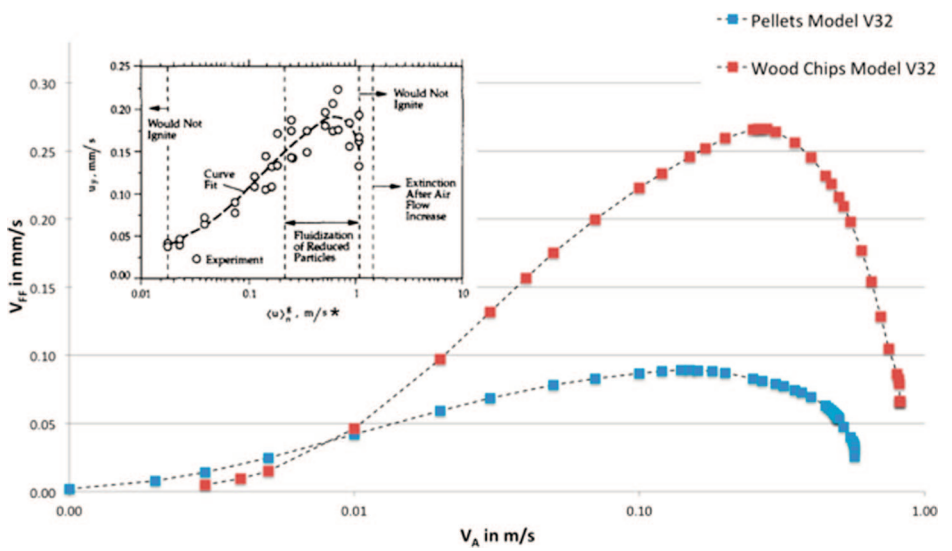

Figure 4: Flame front speed v_{FF} in mm/s against free flow process air speed v_A in m/s. Direct comparison between published, experimental results from [7] (see *, upper left corner) and model results, derived from runs with parameter sets for pellets (blue) and wood chips (red). Single particle model results are scaled by one constant fitting parameter only

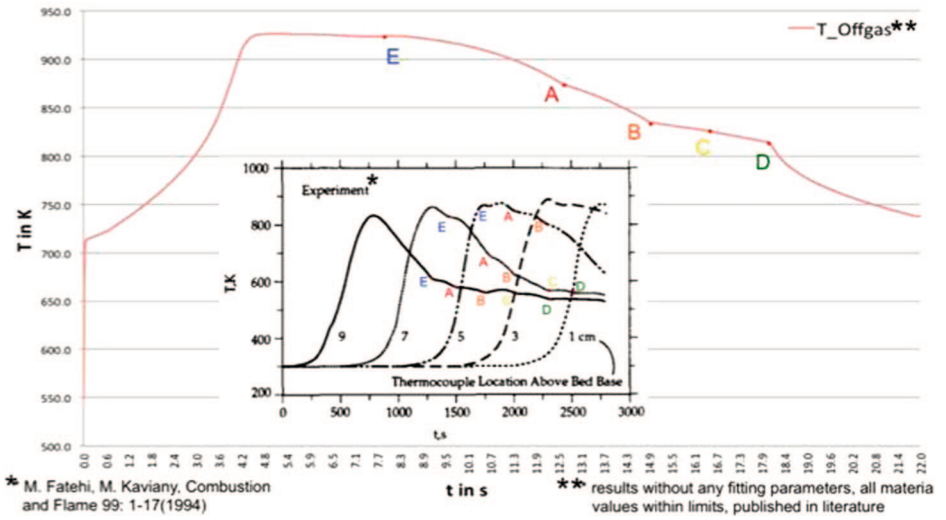

Figure 5: Modeled results of wood gas temperature, T in K, against time, t in s, (pink line) in direct comparison to temperature curves, recorded at counter current gasifier, published in [7]. Spots of unsteady temperature evolution ("E", "A", "B", "C" and "D") do correspond qualitatively

temperature values over process time (see Figure 5). At close examination, those temperature curves reveal five distinct spots of unsteadiness each. They shall hereby be marked as spots "E", "A", "B", "C" and "D" chronologically. It is obvious that these spots mark separate events, which tend to occur independently within each layer of fuel particles in the packed bed.

It can be shown, that those five *spots of unsteady temperature evolution*, can be reproduced by the model and can thus be explained! Figure 5 provides a direct comparison between measured and modeled results.

3.3 INTERPRETATION OF UNSTEADINESS IN TEMPERATURE CURVES

After finding a remarkable, qualitative correspondence between published experiments and modeled results, regarding spots of *unsteady temperature evolution* against time, the model can now be used to explain those phenomena.

Upon examination of additional simulation data, it can be found, that the unsteadiness in spots "A", "B", "C" and "D" (as seen in Figure 5) can be explained by additionally plotting the gas production rates over time, as shown in Figure 6. This way it becomes evident that, whenever the wood gas mixture runs out of a reducing component, a "bump" in the temperature curve occurs. Hence it can be concluded that at such a spot, a higher, finite stage of oxidation of the local wood gas mixture is reached. Spots "A", "B", "C" and "D" correspond to the mixture running out of non-reacting pyrolysis gas (TARs), CH_4, CO and H_2 respectively.

In addition to that, the model shows that the temperature curve behaves unsteadily in spot "E" (see Figure 5), because from here, the *coal phase* starts to act as an effective heat capacity.

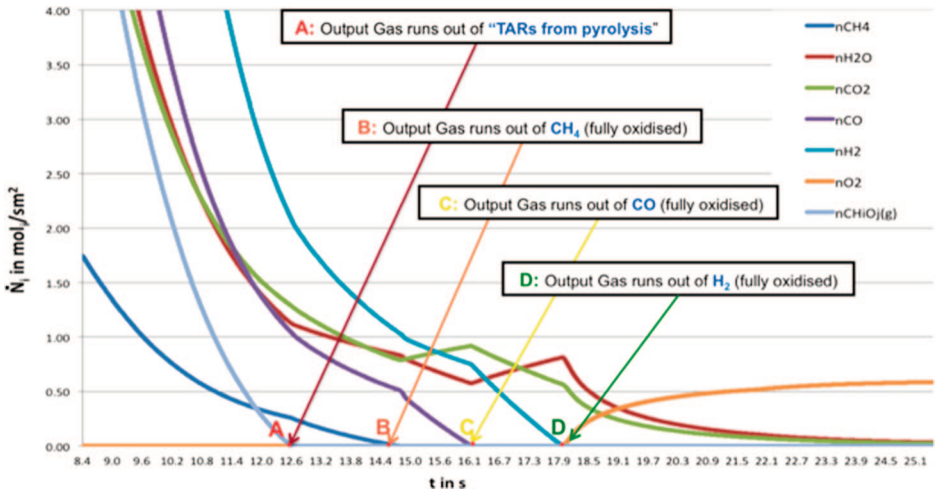

Figure 6: Modeled gas production rates of species i, $\dot{N}_i$ in mol_i/sm^2, against time, t in s. The correspondence of finite oxidation stages of the wood gas mixture, with spots of unsteady temperature evolution "A", "B", "C" and "D" in Figure 5 is highlighted

4. CONCLUSION AND OUTLOOK

The presented 1D, compact, thermo fluid dynamic, single particle gasification and combustion model, has been validated to yield good, qualitative correspondence to reactor scale experiments. While not giving full quantitative results, the model can still be used to provide solid guidelines on how to adapt certain process parameters of a gasifier in direct response to potentially varying fuel input parameters.

A capability to handle additional effects, such as drying, non-sphericity or particle heat-up behavior will be included in future versions of the model.

Furthermore a merging of the gasification model with an adapted version of an OpenFOAM® based, non-spherical, LaGrangian, large particle solver, described in [15], [16, 17] and [18], is intended in the near future. The development of such a solver would entail the possibility to represent e.g. pellets by 3D, non-spherical, LaGrangian particles, within a Eulerian framework. The latter could then be set up based on the thermo- fluid dynamic implementations, elaborated within this paper.

REFERENCES

[1] T.B. Reed, M. Markson (2009). A Predictive Model for Stratified Downdraft Gasification, *Progress in Biomass Conversion, Academic Press, New York;* Vol.4, (1983), pp. 217–254.

[2] A. Anca-Couce, N. Zobel, (2012). Numerical analysis of a biomass pyrolysis particle model: Solution method optimized for the coupling to reactor models, Berlin Institute of Technology, Department of Energy Engineering, Technologies for Renewable Energies, Germany. *Fuel*; Vol.97 (2012) 80–88.

[3] F.V. Tinaut, A. Melgar, J.F. Peerez, A. Horillo (2008). Effect of biomass particle size and air superficial velocity on the gasification process in a downdraft fixed bed gasifier. An experimental and modelling study, School of Engineering, University of Valladolid, Spain, Engineering Faculty, University of Antioquia, Colombia, CIDAUT Research

and Development Center in Transport and Energy, Spain. *Fuel Processing Technology*; Vol.89, (No.11), November 2008, pp. 1076–1089.

[4] Ch. Bruch (2001). *Beitrag zur Modellierung der Festbettverbrennung in automatischen Holzfeuerungen*. PhD thesis. Eidegenoessische technische Hochschule Zuerich, Switzerland, Diss. ETH Nr. 14040, 2001.

[5] N. Prakash, T. Karunanithi (2008). Kinetic Modeling in Biomass Pyrolysis – A Review, Department of Chemical Engineering, Annamalai University, Annamalai Nagar. INSInet Publication, *Journal of Applied Sciences Research*; Vol.4, (No.12): 1627–1636, 2008.

[6] S. Shabbar, I. Janajreh, (2012). Thermodynamic equilibrium analysis of coal gasification using Gibbs energy minimization method, Masdar Institute of Science and Technology (MIST), Abu Dhabi. *Energy Conversion and Management*; Vol.65, (2013), 755–763.

[7] M. Fatehi, M. Kaviany, (1994). Adiabatic Reverse Combustion in a Packed Bed, Department of Mechanical Engineering and Applied Mechanics, University of Michigan. *Combustion and Flame*; Vol.99, (1994), 1–17.

[8] M. C. Melaaen (1996). Numerical analysis of heat and mass transfer in drying and pyrolysis of porous media. Telemark Institute of Technology, Norway. *Numerical Heat Transfer, Part A: Applications;* 29:4, 331–355.

[9] A. Galgano, C. Di Blasi, (2004). Modeling the propagation of drying and decomposition fronts in wood, Dipartimento di Ingeneria Chimica, Universita degli Studi di Napoli. *Combustion and Flame*,;Vol.139, (2004), 16–27.

[10] Ludwig Prandtl, *Fuehrer durch die Stroemungslehre*, Vieweg Verlag, H. Oertel (Hrsg.) 2002.

[11] G. Job, F. Herrmann, (2005). Chemical potential – a quantity in search of recognition, Institut fuer Physikalische Chemie, Universitaet Hamburg, Abteilung fuer Didaktik der Physik, Universitaet Karlsruhe. *European Journal of Physics*; Vol.27, (2006), 353–371.

[12] S. Jarungthammachote, A. Dutta, (2008). Equilibrium modeling of gasification: Gibbs free energy minimization approach and ist application to spouted bed and spout – fluid bed gasifiers, Energy Field of Study, School of Environment, Resources and Development, Asian Institute of Technology, Thailand. *Energy Conversion and Management*, 01/2008; DOI:10.1016/j.enconman.2008.01.006;

[13] S. Gordon, B.J. McBride, (1994). *Computer Program for Calculation of Complex Chemical Equilibrium Compositions and Applications*, I.Analysis, Sanford Gordon and Associates, Cleveland Ohio, Lewis Research Center, Cleveland, Ohio. NASA Reference Publication 1311, 1994.

[14] B.J. McBride, S. Gordon, M.A. Reno, (1993). *Coefficients for Calculating Thermodynamic Transport Properties*, Lewis Research Center, Cleveland, Ohio, Sanford Gordon and Associates, Cleveland Ohio, Heidelberg College, Triffin, Ohio. NASA Technical Memorandum 4513, 1993.

[15] M. Mataln, G.Boiger, W. Brandstätter, B. Gschaider, (2008). Simulation of Particle Filtration Processes in Deformable Media, Part 1: Fluid-Structure Interaction, ICE Stroemungsforschung GmbH., Montanuniversitaet Leoben. *Int.Journal of Multiphysics*, Vol.2, (No.2), July 2008, pp. 179–189(11).

[16] G. Boiger, M. Mataln, W. Brandstätter, B. Gschaider, (2008). Simulation of Particle Filtration Processes in Deformable Media, Part 2: Large Particle Modelling, ICE Stroemungsforschung GmbH., Montanuniversitaet Leoben. *Int.Journal of Multiphysics*, Vol.2, (No.2), July 2008, pp. 191–206(16)8.

[17] G. Boiger, M. Mataln, W. Brandstätter, (2009). Simulation of Particle Filtration Processes in Deformable Media, Part 3.1: Basic concepts and particle-fluid force implementation of a non- spherical dirt particle solver, ICE Stroemungsforschung GmbH., Montanuniversitaet Leoben. *Int.Journal of Multiphysics,* Vol.3, (No.4), March 2010, pp. 407–232(26).

[18] G. Boiger, M. Mataln, W. Brandstätter, (2009). Adaptive time stepping for explicit Euler implementation of spherical and non-spherical particle speed up. ICE Stroemungsforschung GmbH., Montanuniversitaet Leoben. *Int.Journal of Multiphysics;* Vol.3, (No.3), August 2009, pp. 267–291(25).

[19] C. Di Blasi, (2009). Combustion and gasification rates of lignocellulosic chars. Dipartimento di Ingeneria Chimica, Universita degli Studi di Napoli. *Progress in Energy and Combustion Science*; Vol.35, (2009), 121–140.

[20] K.W. Ragland, D.J. Aerts, (1990). Properties of Wood for Combustion Analysis. Department of Mechanical Engineering, University of Wisconsin-Madison. *Bioresource Technology*; Vol.37, (1991), 161–168.

[21] *IUPAC Compendium of Chemical Terminology (the "Gold Book")*. doi:10.1351/goldbook.A00446 (Version: 2.3.1).